The Diabatic Picture of Electron Transfer, Reaction Barriers, and Molecular Dynamics

Troy Van Voorhis, Tim Kowalczyk, Benjamin Kaduk, Lee-Ping Wang, Chiao-Lun Cheng, and Qin Wu*

Department of Chemistry, Massachusetts Institute of Technology, Cambridge, Massachusetts 02139; email: tvan@mit.edu

* Present Address: Center for Functional Nanomaterials, Brookhaven National Laboratory, Upton, New York 11973

Annu. Rev. Phys. Chem. 2010. 61:149–70

First published online as a Review in Advance on November 13, 2009

The *Annual Review of Physical Chemistry* is online at physchem.annualreviews.org

This article's doi: 10.1146/annurev.physchem.012809.103324

0066-426X/10/0505-0149$20.00

Key Words

reaction dynamics, nonadiabatic, density functional

Abstract

Diabatic states have a long history in chemistry, beginning with early valence bond pictures of molecular bonding and extending through the construction of model potential energy surfaces to the modern proliferation of methods for computing these elusive states. In this review, we summarize the basic principles that define the diabatic basis and demonstrate how they can be applied in the specific context of constrained density functional theory. Using illustrative examples from electron transfer and chemical reactions, we show how the diabatic picture can be used to extract qualitative insight and quantitative predictions about energy landscapes. The review closes with a brief summary of the challenges and prospects for the further application of diabatic states in chemistry.

1. INTRODUCTION

Adiabatic state: an eigenstate of the Born-Oppenheimer electronic Hamiltonian

Diabatic state: an electronic state that does not change character as a function of molecular geometry

ET: electron transfer

CDFT: constrained density functional theory

Qualitatively, a diabatic electronic state is one that does not change its physical character as one moves along a reaction coordinate. This is in contrast to the adiabatic, or Born-Oppenheimer, electronic states, which change constantly so as to remain eigenstates of the electronic Hamiltonian. A classic example of the interplay between diabatic and adiabatic pictures is sodium-chloride dissociation (**Figure 1**). Here, the ground adiabatic state is thought of as arising from the avoided crossing between an ionic and a covalent state. The adiabatic state thus changes character—transforming from Na-Cl to Na^+-Cl^- as the bond gets shorter—whereas the ionic and covalent configurations play the role of diabatic states.

Diabatic electronic states play a role in a variety of chemical phenomena but are, at the same time, underappreciated by many chemists. For example, diabats are often used in the construction of potential energy surfaces because they are smooth functions of the nuclear coordinates (1–3). In spectroscopy, diabatic states are invoked to assign vibronic transitions and rationalize the rates of interstate transitions (4–6). In the general description of electronically excited dynamics, diabatic states are advantageous because they typically have a small derivative coupling, simplifying the description of electronic transitions (7–11). In scattering theory, diabatic states connect to clearly defined product channels (12–14). Finally, diabatic states play a qualitative role in our understanding of molecular bonding (15–17) (as illustrated by the NaCl example above), electron transfer (ET) (18, 19), and proton tunneling (20–22).

This review article is intended as an introduction to the basic concepts behind the construction of diabatic states and their use in describing chemical phenomena. After summarizing different definitions of diabatic states—and in particular discussing why so many competing definitions exist—we focus on a particular definition based on constrained density functional theory (CDFT). We show how CDFT-derived diabatic states are computed in practice and discuss several illustrative chemical applications.

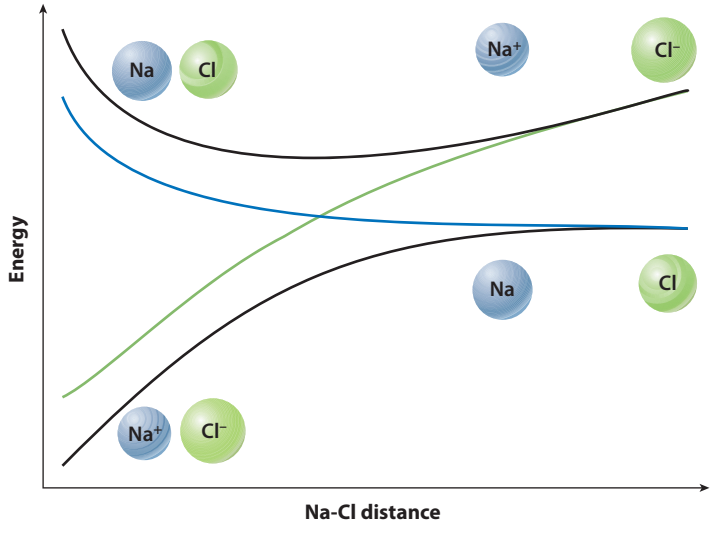

Figure 1

NaCl dissociation in the diabatic and adiabatic representations. The ionic (*green*) and covalent (*blue*) diabatic states maintain the same character across the potential energy surface, whereas the adiabatic states (*black*) change.

2. STRICT DIABATS CANNOT BE OBTAINED FROM ADIABATS

Of central importance to the study of diabatic electronic states is the idea of a strictly diabatic basis (SDB) (23). By definition, for a set of strict diabats, $|\Phi_i\rangle$, the derivative coupling between any two states vanishes at every possible nuclear configuration, **R**:

$$\mathbf{d}_{ij}(\mathbf{R}) \equiv \left\langle \Phi_i \left| \frac{\partial}{\partial \mathbf{R}} \Phi_j \right. \right\rangle = 0 \quad \forall i,\ j,\ \mathbf{R}. \tag{1}$$

This definition is in line with our qualitative idea that diabatic states do not change when the nuclei move (i.e., the derivative is zero). Given an arbitrary set of M adiabatic states, $|\Psi_i\rangle$ (e.g., a few important electronic states involved in a photochemical reaction), it would clearly be desirable to develop a formula for a set of M strictly diabatic states that span the same Hilbert space as the given adiabats. That is to say, one would like to have a set of orthonormal states that satisfy Equation 1 and for which

$$|\Phi_i(\mathbf{R})\rangle = \sum_j A_{ij}(\mathbf{R})|\Psi_j(\mathbf{R})\rangle \tag{2}$$

for some matrix **A**. The matrix **A** is called the adiabatic-to-diabatic transformation matrix, for obvious reasons (24, 25).

If states of this form could be obtained, they would clearly provide the most rigorous definition of diabatic states; one would simply need to specify the set of interesting adiabatic states, and then the corresponding diabatic states could be automatically determined. Unfortunately it is not generally possible to create an SDB from a given adiabatic basis (23) (see the sidebar).

This result has a significant impact on how we approach diabatic states. One has the common situation in which there is an ideal mathematical construction for diabatic states (SDBs) but no way of realizing this ideal in practice. Thus, if one wants diabatic states for a particular application,

PROOF THAT ONE CANNOT CREATE A STRICTLY DIABATIC BASIS FROM A GIVEN ADIABATIC BASIS

First write down the nonadiabatic coupling between the adiabatic states

$$\tau_{ij}(\mathbf{R}) \equiv \left\langle \Psi_i(\mathbf{R}) \left| \frac{\partial}{\partial \mathbf{R}} \Psi_j \right. \right\rangle. \tag{3}$$

It is important to note that once the adiabatic states have been chosen, τ is fixed and cannot be changed. Now, write Equation 1 in terms of τ and **A**:

$$\left\langle \Phi_i \left| \frac{\partial}{\partial \mathbf{R}} \Phi_j \right. \right\rangle = \mathbf{A}^\dagger \tau \mathbf{A} + \mathbf{A}^\dagger \nabla \mathbf{A} = 0$$
$$\rightarrow \tau \mathbf{A} + \nabla \mathbf{A} = 0, \tag{4}$$

which can be considered the condition that determines the correct **A** once the couplings are known (24, 25). We now take the derivatives of Equation 4 with respect to **R**. After some manipulation, and exploiting the fact that mixed partial derivatives must be the same independent of the order in which they are taken, we obtain

$$\nabla \times \tau = \tau \times \tau. \tag{5}$$

This relationship is called the curl condition, and it specifies a restriction that must be satisfied by τ if one hopes to construct an SDB out of the given set of adiabatic states. Unfortunately, this condition is not satisfied for the Born-Oppenheimer eigenstates of real molecules, except under rare circumstances (23, 26).

one must weaken the search criteria in one of two ways. One either looks for weakly diabatic states (i.e., ones that almost satisfy Equation 5) that span a given adiabatic space, or one looks for strictly diabatic states that almost span the desired space. One expects that approximate diabats will be good descriptors of chemistry insofar as they faithfully reproduce the strict diabats, and the approximations can be made better and better if one allows more and more states.

3. STRATEGIES FOR OBTAINING DIABATIC STATES

Given the results of the previous section, it is clear that we will need to make approximations to obtain practical diabatic states. As a rule, theoretical chemists enjoy making approximations, and thus it comes as no surprise that we have many subtly different ways of obtaining diabatic states for real systems. Broadly, these approaches can be broken down into two categories: techniques that try to deduce the best set of diabatic states from a given set of adiabats and those that attempt to construct diabatic states directly. The emphasis of this review is constructive methods, but to understand these techniques in context, we briefly summarize the most popular alternatives.

3.1. Deductive Strategies

Given a set of adiabats, there are a number of methods that can be employed to obtain approximate diabats.

Minimize the coupling. If one cannot entirely remove the derivative couplings between diabatic states (Equation 1), then an obvious strategy is to try to make the couplings as small as possible—typically in a local sense. The original proposal along these lines is due to Baer (24, 25), who proposed picking an arbitrary set of diabatic states at a reference point, $\mathbf{R}_0$, and then integrating Equation 4 along a path (e.g., a reaction path) to obtain states that locally are strict diabats. This procedure turns out to be quite computationally demanding, in part because it requires the derivative couplings at every point.

Slowly varying states. Often one is looking for diabatic states that simply do not change much from one point to another. The best established method in this family is the block diagonalization (BD) approach (27). Here, one performs a unitary rotation in configuration space that block diagonalizes the electronic Hamiltonian, while leaving a target set of diabatic states as similar as possible to a reference set of states (28, 29). This procedure has the benefit that it minimizes the ℓ^2 norm of the derivative coupling ($|\mathbf{d}|^2 = \min$) in the vicinity of the reference point (30). Other techniques in the same spirit include enforcing configurational uniformity, so that each diabatic wave function is predominantly constructed from a fixed set of electronic configurations (31, 32); regularizing adiabatic states to remove the divergent portion of the coupling (33, 34); and the fourfold way, which combines many of the positive features of the above methods (35, 36). As a starting point, these techniques require highly accurate adiabatic states and are thus typically used in conjunction with high-level configuration interaction (CI) calculations.

Eigenstates of a physical observable. By far the oldest form of diabatization is the Mulliken-Hush approach (37, 38) to ET. Here, the approximate diabatic states are defined using purely spectroscopically observable information (transition energy, transition dipole μ_{12}, and change in dipole $\Delta\mu$). This approach can be generalized to deal with multiple states in a way that only involves adiabatic quantities (39, 40) if one defines the diabatic states as the eigenstates of the dipole moment operator (39, 41). Similarly, multiple charge centers and/or excitation energy transfer can

be dealt with by defining the diabatic states to be the maximally localized wave functions in real space (42, 43). In each case, one realizes that the eigenstates of any fixed physical observable (such as the dipole or localization) will not change much as molecules rearrange, and thus they will form a transferable set of diabatic states. Although computationally convenient, these techniques are typically only applied to electron- and energy-transfer problems.

VB: valence bond

FAAQ: formanilide-anthraquinone

3.2. Constructive Strategies

In this family of approaches, the diabatic states are constructed directly without reference to any particular adiabats.

Valence bond theory. Although not widely publicized, Pauling's idea of resonance structures within valence bond (VB) theory (15) provides a natural definition of diabatic states (44, 45). For example, bonding in NaCl involves two resonance structures—$|Na^+\ Cl^-\rangle$ and $|Na : Cl\rangle$—which clearly have diabatic character from an ET perspective. The allyl radical has two structures—$|CH_2 = CH - \dot{C}H_2\rangle$ and $|\dot{C}H_2 - CH = CH_2\rangle$—that place the double bond in a fixed location irrespective of which C–C bond is actually shorter. The VB-diabatic connection has been used to describe S_N1 reactions (46) and proton-coupled ET (47), and is the basis for the molecular orbital VB (48) and empirical VB (16, 17) methods. It is important to realize that, to obtain accurate diabatic states (i.e., to obtain diabatic states that can faithfully reproduce the lowest several adiabats), it is often desirable to include more than the minimal number of diabatic states suggested by chemical intuition (49).

Density constraints. In many cases, diabatic states can be clearly identified based on their density—ionic states such as $|D^+\ A^-\rangle$ will have excess electron density on one side of the molecule, whereas a covalent state such as $|D^{\uparrow}\ A^{\downarrow}\rangle$ will have excess spin density on one side. Thus, suitable diabatic states can be obtained by optimizing the wave function subject to a constraint on the density. This concept is the basis of the frozen density functional method (50, 51) as well as the CDFT approach (52) detailed in the following section. Applying constraints is conceptually simpler than decomposing the wave function in terms of VB states, but this approach can be computationally more challenging as it requires separate self-consistent calculations for each diabatic state.

4. CONSTRAINED DENSITY FUNCTIONAL THEORY OF DIABATIC STATES

As a concrete example, we now focus on the specific choice of using density constraints to define diabatic states and outline the steps that must be taken to represent the electronic Hamiltonian, $\mathbf{H_{el}}$, in the constrained diabatic basis.

4.1. Obtaining Diabatic States

By definition, we choose each diabatic state to be the lowest energy state of the system subject to a constraint on the density. For concreteness, it is good to have an example in mind, and we use the $|D^+\ A^-\rangle$ state of the formanilide-anthraquinone (FAAQ) molecule (**Figure 2**) as an illustration. This particular charge-transfer excited state has been identified spectroscopically as having a very long lifetime (>900 μs) in DMSO solution (53).

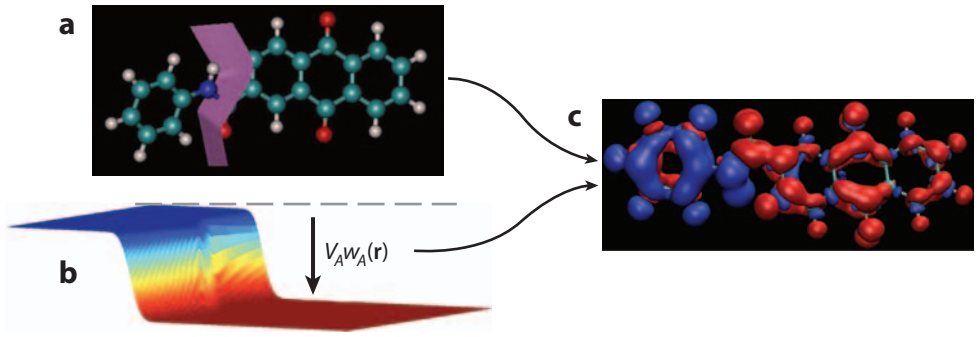

Figure 2

Obtaining the $D^+ A^-$ state of FAAQ. (*a*) One chooses which atoms belong to the acceptor. The atomic partition operator then divides space between the fragments, as illustrated by the dividing surface. (*b*) A constraint potential is applied. Changing the Lagrange multiplier changes the depth of the potential and controls the net charge on the acceptor. (*c*) A ground-state calculation in the presence of the optimal potential results in exactly one excess electron (*red*) on the acceptor and one excess hole (*blue*) on the donor.

Step 1: fragment selection. One must define a group of atoms whose charge/spin/electronic state one wants to constrain. Typically, this is done by chemical intuition, so that in the case of FAAQ, aniline (C_6H_5NH) is identified as the donor, whereas anthraquinone ($COC_{14}H_7O_2$) is the acceptor.

Step 2: defining the constrained observable. In practice, there are any number of physical observables that one might constrain to create diabatic states (e.g., the dipole moment, the magnetic moment, the local spin state). In the case of a charge-transfer state, the obvious thing to constrain is the fragment charge (54). But how do we define the fragment charge? Mulliken (55), Löwdin (56), Bader (57), Becke (58), and Hirshfeld (59) populations all provide useful but nonunique prescriptions for partitioning charge among different atoms within a molecule. For practical purposes, one must make an arbitrary choice at this stage and verify later that this choice does not materially affect the predictions. To this end, we choose Becke's partitioning wherein the charge on the acceptor is given by

$$N_A = \int w_A(\mathbf{r})[\rho^\alpha(\mathbf{r}) + \rho^\beta(\mathbf{r})]d\mathbf{r} \equiv \int w_A(\mathbf{r})\rho(\mathbf{r})d\mathbf{r}, \quad (6)$$

where ρ is the electron density, and w_A is the Becke weight operator that determines the charge on the acceptor. By design, $w_A(\mathbf{r})$ is nearly unity in regions of space near the acceptor, and nearly zero in regions of space near the donor (58) (see **Figure 2**). For the case of FAAQ, one clearly wants $N_A = 1.0$ so that the net charge on the acceptor is -1. At the end of the calculations of step 3, this choice leads to the lowest energy state such that the Becke partial charges of all the atoms in the acceptor sum to precisely -1.0.

Step 3: constrained minimization. To obtain the lowest energy state subject to the constraint in Equation 6, one introduces a Lagrange multiplier, V_A, and looks for the stationary point of

$$W[\rho, V_A] = E[\rho] + V_A\left(\int w_A(\mathbf{r})\rho(\mathbf{r})d\mathbf{r} - N_A\right), \quad (7)$$

where $E[\rho]$ is the electronic energy one is trying to minimize. This formalism could be applied to coupled-cluster, reduced density matrix, or many-body perturbation theory energy functions (60).

However, in Equation 7, we specialize to the case of DFT both because it is relatively fast and because in principle it can give the exact energy of the system under any density constraint (52). The stationary condition for V_A ($\frac{\partial W}{\partial V_A} = 0$) just enforces the constraint (Equation 6). Meanwhile, in a Kohn-Sham (KS) framework, the stationary condition with respect to the density gives a Schrödinger equation for the KS orbitals:

$$\left(-\frac{1}{2}\nabla^2 + \int \frac{\rho(\mathbf{r}')}{|\mathbf{r}-\mathbf{r}'|}d\mathbf{r}' + v_{xc}(\mathbf{r}) + V_A w_A(\mathbf{r})\right)\psi_i(\mathbf{r}) = \epsilon_i \psi_i(\mathbf{r}), \tag{8}$$

where v_{xc} is the exchange-correlation potential and ψ_i are the KS orbitals. Thus we see that the Lagrangian introduces an additional constraint potential, $V_A w_A(\mathbf{r})$, that controls the charge on the acceptor (see **Figure 2**). The optimal value of V_A is determined implicitly: The correct value of V_A modifies the KS equations in such a way that the resulting density ($\rho(\mathbf{r}) \equiv \sum_i |\psi_i(\mathbf{r})|^2$) satisfies Equation 6. Because the implicit optimization is strictly a maximization, the simultaneous optimization of ρ and V_A can be accomplished in a similar amount of time to a standard ground-state DFT calculation (60, 61). Thus, in this constrained scheme, the diabatic states are obtained as adiabatic ground states of the system under an alternative potential.

This prescription can be simply generalized to deal with charge (54, 60, 61) and/or spin (62–65) constraints on an arbitrary number of fragments. We have implemented the above three-step procedure into the NWChem (66) and Q-Chem (67) program packages. The result is that the user can specify not only the positions of the atoms, but also the charge and spin on any selected groups of atoms within the molecule. The fact that these are modified ground-state calculations facilitates analytic force evaluation (54) as well as seamless integration into quantum mechanics/molecular mechanics and continuum electrostatic models of solvation.

Applying these steps to obtain both neutral ($|\mathrm{D\,A}\rangle$) and charge-transfer ($|\mathrm{D^+\,A^-}\rangle$) configurations for FAAQ using B3LYP (68) in the 6-31G* basis and COSMO (69) to describe solvation in DMSO, we find a relaxed charge-transfer energy $\Delta G = 2.31$ eV, which is in excellent agreement with the experimental measurement of 2.24 eV (53, 54). Thus, constraints can be a quantitative tool for obtaining diabatic states in realistic molecules.

Density functional theory (DFT): a means of determining the ground-state properties as a functional of the electron density

Diabatic coupling: the matrix element of the electronic Hamiltonian between two different diabats: $V_{ij} = \langle \Psi_i | \hat{H}_{el} | \Psi_j \rangle$

4.2. Computing the Diabatic Coupling

In the diabatic basis, the couplings, $V_{ij} = \langle \Psi_i | \hat{H} | \Psi_j \rangle$, play an analogous role to the derivative couplings in the adiabatic basis—both terms determine the rate of transitions between electronic states—but the diabatic couplings have the advantage of not requiring wave-function derivatives. An accurate, simple expression for the diabatic coupling is particularly important because there are no quasi-classical formulas for V_{ij}. For example, the diabatic energies can quite often be estimated using classical expressions such as the Rehm-Weller equation (70). At the same level of theory, V_{ij} arises purely from quantum tunneling—the exponential tail of the donor wave function overlaps with the acceptor and vice versa—which has no classical counterpart. Thus, the diabatic coupling depends sensitively on the distance between the interacting fragments and their relative orientations, and a complete picture depends crucially on estimating it (71, 72).

V_{ij} also allows us to completely specify $\mathbf{H_{el}}$ in the diabatic basis. For example, for two diabatic states,

$$\mathbf{H_{el}} \equiv \begin{pmatrix} E_1 & V_{12} \\ V_{12} & E_2 \end{pmatrix}. \tag{9}$$

The energies, E_i, can be obtained directly from CDFT, and only V_{12} is unknown. We note that, because they are eigenstates of different Hamiltonians, the pure constrained states are not orthogonal ($\langle \Psi_1 | \Psi_2 \rangle \equiv S \neq 0$). If one is interested in the diabatic coupling itself, physical intuition

dictates that some orthogonal set of diabatic states is required—otherwise the overlap between the wave functions is interpreted as a spurious coupling. A unique orthogonalization arises if all the diabatic states are specified by different average values of the same partition operator, $\hat{w}$ (e.g., if all the diabats have distinct charge/spin states for a single fragment within the molecule). In this case, one can look for the generalized eigenvectors, $\mathbf{d}$, of the partition operator via $\mathbf{Wd} = n\mathbf{Sd}$ and then transform the Hamiltonian to the orthogonal basis: $\mathbf{H} \rightarrow \mathbf{d}^{\dagger}\mathbf{Hd}$. For clarity, we refer to the coupling in the nonorthogonal basis as V_{ij}, whereas for the orthogonal coupling, we use H_{ij}. In either case, the adiabatic states are defined by the generalized eigenequation

$$\mathbf{Hc} = \begin{pmatrix} E_1 & V_{12} \\ V_{12} & E_2 \end{pmatrix} \begin{pmatrix} c_1 \\ c_2 \end{pmatrix} = \epsilon \begin{pmatrix} 1 & S \\ S & 1 \end{pmatrix} \begin{pmatrix} c_1 \\ c_2 \end{pmatrix} \equiv \epsilon \mathbf{Sc}. \tag{10}$$

In the present context, the challenge in computing $\langle \Psi_i | \hat{H} | \Psi_j \rangle$ using CDFT is that DFT only gives us access to the energy and density of each diabatic state—the wave function is never constructed. Hence, we need to make an approximation to evaluate V_{ij} in CDFT. Toward this end, we note that for constrained diabatic states, each diabat (i) is an eigenstate of the Hamiltonian in its own alternative potential ($V_i \hat{w}_i$):

$$\hat{H} + V_i \hat{w}_i | \Psi_i \rangle \equiv \hat{H}_i | \Psi_i \rangle = F_i | \Psi_i \rangle \equiv (E_i + V_i N_i) | \Psi_i \rangle \quad \forall i, \tag{11}$$

where E_i, V_i, and N_i are the diabatic energy, associated Lagrange multiplier, and specified constraint value, respectively, for the i-th diabat—all of which are provided directly by CDFT. This allows us to rewrite the diabatic coupling in the suggestive form (73):

$$\langle \Psi_i | \hat{H} | \Psi_j \rangle = \frac{1}{2} \langle \Psi_i | \hat{H}_i - V_i \hat{w}_i + \hat{H}_j - V_j \hat{w}_j | \Psi_j \rangle = \frac{F_i + F_j}{2} \langle \Psi_i | \Psi_j \rangle - \frac{1}{2} \langle \Psi_i | V_i \hat{w}_i + V_j \hat{w}_j | \Psi_j \rangle. \tag{12}$$

Thus, the many-body matrix elements of $\hat{H}$ in the diabatic basis can be reduced to a combination of zero-body (i.e., wave-function overlap) and one-body (constraint potential) matrix elements. Equation 12 contains the physical insight that the coupling between diabats only depends on the overlap between them (first term) and the potential required to create them (second term).

At this stage, we make an approximation and use the KS determinants $|\Phi_i\rangle$ in place of the exact diabatic states $|\Psi_i\rangle$ in Equation 12. This is certainly an approximation, but it is one that can work surprisingly well in practice (73). For example, if we examine hole transfer in the mixed valence system Zn_2^+ as a function of the Zn-Zn distance, we expect that the tunneling matrix element will decay exponentially (40). Using B3LYP and a large basis (40, 74), one finds values for H_{ij} that differ by <150 cm^{-1} from the corresponding BD predictions for $5\,\text{Å} < R < 9\,\text{Å}$ (40). The differences can largely be attributed to the underlying electronic structure—the BD uses CASSCF, whereas the CDFT results use B3LYP. Thus the present prescription for H_{ij} appears to be adequate for the coupling of well-separated fragments.

5. APPLICATIONS

5.1. Electron Transfer

Diabatic states play a critical role in ET theory (see **Figure 3**) (19, 75). One first posits the existence of reactant and product diabatic states where the electron is localized on the donor and acceptor, respectively. Reactions are then typically characterized by the thermodynamic driving force, ΔG, and the reorganization energy, λ, of the diabatic free-energy surfaces. The latter quantity measures the stiffness of the molecular framework, which can often be inferred from the Stokes shift of the

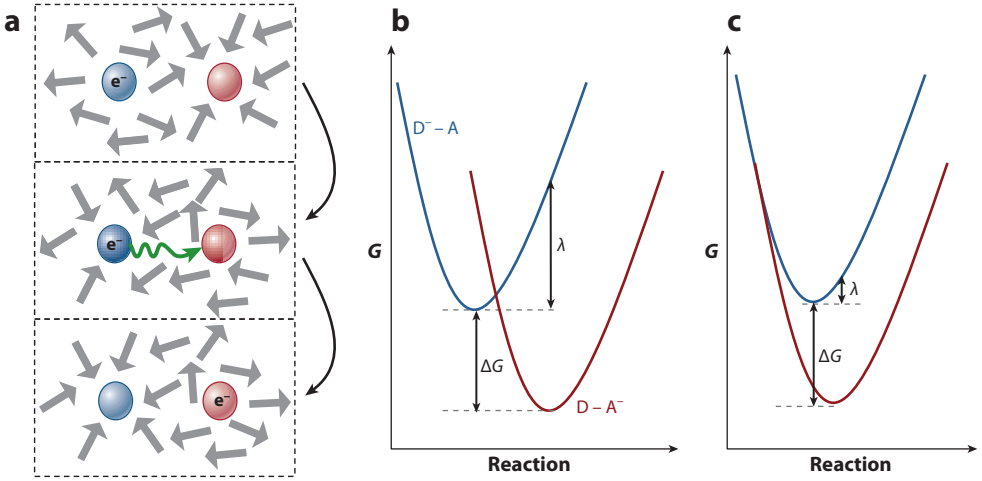

Figure 3

(*a*) In solution, the electron-transfer reaction coordinate is dominated by solvent reorganization. The free-energy landscape can be characterized by the driving force (ΔG), measuring the energy released, and reorganization (λ), measuring the structural relaxation energy. (*b*) If $\Delta G < \lambda$, the reaction is in the normal regime, and the rate increases with ΔG. (*c*) If $\Delta G > \lambda$, the reaction is in the inverted regime, and the rate decreases with increasing ΔG.

charge-transfer absorption/emission bands (76). If we assume that the free-energy surfaces are perfect parabolas with the same curvature (equivalent to the assumption that the system responds linearly), it is easy to work out that the activation energy for ET is $\Delta G^{\ddagger} = (\Delta G + \lambda)^2/4\lambda$ leading to a rate (77, 78)

$$k_{ET} \propto |H_{DA}|^2 \frac{1}{\sqrt{4\pi\lambda kT}} e^{-\Delta G^{\ddagger}/kT} = |H_{DA}|^2 \frac{1}{\sqrt{4\pi\lambda kT}} e^{\frac{-(\Delta G+\lambda)^2}{4\lambda kT}}. \quad (13)$$

There are many generalizations of this simple formula that account for anharmonic free-energy surfaces (79), adiabatic ET (80), and quantum nuclear effects (81). In the present article, we are interested in a more basic question: Given that Equation 13 or one of its generalizations is appropriate for a given problem, how can one compute accurate diabatic ET states and extract from those states parameters such as ΔG and λ? That is to say, how do we translate the cartoon (**Figure 3**) into a calculation?

We can trace the use of CDFT to answer this question back to Wesolowski & Warshel's (50) idea of using a frozen density to describe the charge distribution of each diabatic state. More recent work has employed CDFT (or the related concept of penalty function DFT) to define the diabatic potential surface, which can then be explored to estimate ΔG and λ (54, 82, 83). To do this, we need to define the reaction coordinate. **Figure 3*a*** illustrates the physical picture (84): When the electron is on the donor (acceptor), the solvent orients to stabilize the electron on the donor (acceptor). The transition state involves a fluctuation of the solvent that untraps the electron and initiates transfer. This picture leads to several reasonable choices for the reaction coordinate: One can choose the equilibrium solvent polarization (84), the fractional degree of ET ($D^{-1+q}\,A^{-q}$) (85), or the energy gap [$\Delta E = E(D^+A^-) - E(DA) \equiv E_D - E_A$] (86) between reactants and products. Below we show a preference toward the last definition, which has certain formal advantages (87).

DCT: dielectric continuum theory

Once the diabatic states have been defined, the key remaining decision for condensed-phase ET concerns the treatment of the solvent. In some sense, the presence of solvent actually validates the use of diabatic states, so some care needs to be taken here (88). Broadly speaking, there are two paths from which to choose: implicit models—in which the solvent is replaced by a fictitious continuous medium—and explicit models—in which many discrete solvent molecules are included in the simulation. To compute $\Delta G \equiv G_D^{eq} - G_A^{eq}$ and $\lambda \equiv G_A^{neq} - G_A^{eq}$, one requires three free energies: (*a*) G_D^{eq}, the equilibrium free energy of the donor state; (*b*) G_A^{eq}, the equilibrium free energy of the acceptor state; and (*c*) G_A^{neq}, the free energy of the acceptor state in the ensemble of nuclear configurations (q_D) most favorable for the donor. The first two are obviously equilibrium properties, whereas G_A^{neq} requires a nonequilibrium Frank-Condon approximation, wherein the nuclear positions are all fixed by the donor ensemble, but the solute and solvent electrons are relaxed in the acceptor electronic state. We now briefly review how these free energies are computed in the presence of solvent.

Implicit solvent. At a basic level, an implicit solvent model has two steps. First, one carves out a spatial cavity around the solute molecule(s). Second, the space outside the cavity is filled with a dielectric medium, which represents the solvent. Because a dielectric can respond to the molecular charge distribution inside the cavity, this prescription provides a crude approximation to the electrostatic interaction between solvent and solute. This dielectric continuum theory (DCT) has a long history within chemistry. In the days before computers, these models were popular primarily because they can provide simple, analytic formulas for the solvation energy of a molecule (80, 84, 89, 90). As time has progressed, these models have become more sophisticated (91–94) so that modern DCT is considered a computational and essentially predictive model of both chemical and biological phenomena.

The advantage of using DCT in describing ET is that it vastly reduces the number of degrees of freedom one must explore because the solvent molecules have been integrated out. Thus, equilibrium free energies such as G_D^{eq} or G_A^{eq} can be computed directly by optimizing the geometry of FAAQ with the electron constrained to be on the donor (D A) or acceptor (D^+ A^-) in the presence of the solvent dielectric. Because analytic gradients of the energy are readily calculated in CDFT, geometry optimizations of this type are straightforward, and the positions of individual solvent molecules need never be considered (54). Applying this prescription to FAAQ using B3LYP/6-31G*/COSMO calculations, we obtain $\Delta G = 2.31$ eV, which, as noted above, is in excellent agreement with experiment ($\Delta G = 2.24$ eV). Similarly, for a ferrocene adduct of FAAQ (Fc-FAAQ), the computed ΔG goes down to 1.02 eV, still in excellent agreement with the experiment at 1.16 eV (53, 54).

To compute λ, one requires G_A^{neq}, which is somewhat tricky to obtain in a continuum model. The difficulty is that, because we have integrated out all the solvent degrees of freedom, it is challenging to freeze the solvent nuclei while allowing the solvent electrons to relax. To overcome this, it is assumed that the solvent dielectric has a fast component ($\epsilon_\infty \approx n_{opt}^2$) arising from electronic polarization, and a total dielectric (ϵ_0), which captures electronic and nuclear response (95). Each dielectric, $\epsilon = \epsilon_\infty$, ϵ_0, interacts with the solute through a reaction field V_0 (91):

$$V_0 = -g(\epsilon_0)V_{\text{solute}} \equiv -\frac{\epsilon_0 - 1}{\epsilon_0} V_{\text{solute}}, \tag{14}$$

where V_{solute} is the potential of the solute on the boundary (*B*) of the cavity (96). From Equation 14, we identify the slow field as

$$V_{\text{slow}} = [g(\epsilon_0) - g(\epsilon_\infty)]V_{\text{solute}}, \tag{15}$$

which simply interprets the slow part as the difference between the total and fast components. To compute G_A^{neq}, then, one first performs a calculation with the electron on the donor and obtains V_{slow}. A calculation is then performed at the same geometry with the electron on the acceptor and two fields: (*a*) a static field of V_{slow} and (*b*) a polarizable continuum with dielectric ϵ_∞. These two fields reflect the nuclear polarization of the solvent (which is frozen) and the electronic polarization (which responds), respectively. Finally, denoting the acceptor electron density and potential by ρ^A, V^A, and similarly for the donor (97),

$$G_A^{neq} \equiv E[\rho^A] - \frac{1}{2}g(\epsilon_\infty)\int_B V^A(\mathbf{r})\rho^A(\mathbf{r})d\mathbf{r} - \int_B V_{\text{slow}}(\mathbf{r})\rho^A(\mathbf{r})d\mathbf{r} + \frac{1}{2}\int_B V_{\text{slow}}(\mathbf{r})\rho^D(\mathbf{r})\,d\mathbf{r}. \quad (16)$$

On the fly: any technique wherein molecular energies and forces are calculated as needed rather than being inferred from precomputed values

If we apply this prescription to FAAQ and Fc-FAAQ using B3LYP/6-31G*/COSMO calculations, we obtain $\lambda_D = \lambda_A = 0.6$ eV for FAAQ and $\lambda_D = \lambda_A = 0.8$ eV for Fc-FAAQ. These results are qualitatively consistent with the experimental observation that FAAQ is in the inverted regime, so that $\lambda \ll \Delta G$, whereas Fc-FAAQ undergoes rapid charge recombination, which implies $\Delta G \approx \lambda$ (53). However, the results are quantitatively incorrect: One infers a value of $\lambda \approx 1.45$ eV from the experimental kinetics, which is much higher than either DCT prediction. The disagreement likely has to do with the fact that modern DCT is heavily parameterized toward equilibrium properties, with relatively less attention paid to the type of nonequilibrium solvation involved here. To obtain more consistent results away from equilibrium, we turn to explicit models.

Explicit solvent. Explicit-solvent models offer manifold advantages over implicit models: One can directly probe reaction dynamics, obtain information about the entire free-energy surface, and obtain parameter-free ab initio predictions of free energies. The downside is that these calculations are 1000 to 1,000,000 times as expensive as their implicit counterparts, and the rapidity with which results can be obtained is thus somewhat hindered. The seminal papers in the field use classical force fields to describe the diabatic potential energy surfaces, in which case the calculations are much faster. These investigations have established rate expressions (98–100), mapped out free-energy surfaces (86, 101), validated the reaction coordinate (102, 103), and predicted qualitative reaction dynamics (85, 104).

More recently, advances in computer speed have opened the possibility of exploring the diabatic ET energy landscape in explicit solvent using DFT (62, 65, 82, 83, 105–110). The general prescription for these simulations is illustrated in **Figure 4**, again for the example of FAAQ in DMSO. First, one performs several long molecular dynamics trajectories for each diabatic state in the presence of solvent to properly sample the energy landscape. These simulations would be virtually impossible using a deductive prescription for the diabatic states—which would require derivatives of excited-state wave functions and/or the identification of a reference structure. For CDFT, one merely requires ground-state energy derivatives to perform the relevant on-the-fly Born-Oppenheimer-like dynamics (54). For example, in the simulations in **Figure 4**, the solvent was modeled by a polarizable force field, and the diabatic states of FAAQ were determined by constrained B3LYP/3-21G. The technical details of the computations can be found elsewhere (110). However, we note that a traditional fixed-charge model of the solvent (as opposed to the polarizable approach used here) would result in severe overestimation of the reorganization energy (110, 111), essentially neglecting all the fast component of the dielectric response.

Once the molecular dynamics simulations are complete, a large number of independent snapshots are collected from the trajectories, and the energy of both diabatic charge states at every snapshot is computed. By performing this procedure for the neutral and charge-transfer trajectories of FAAQ, one obtains the two energy gap distributions displayed in **Figure 4*c*,*d***, respectively.

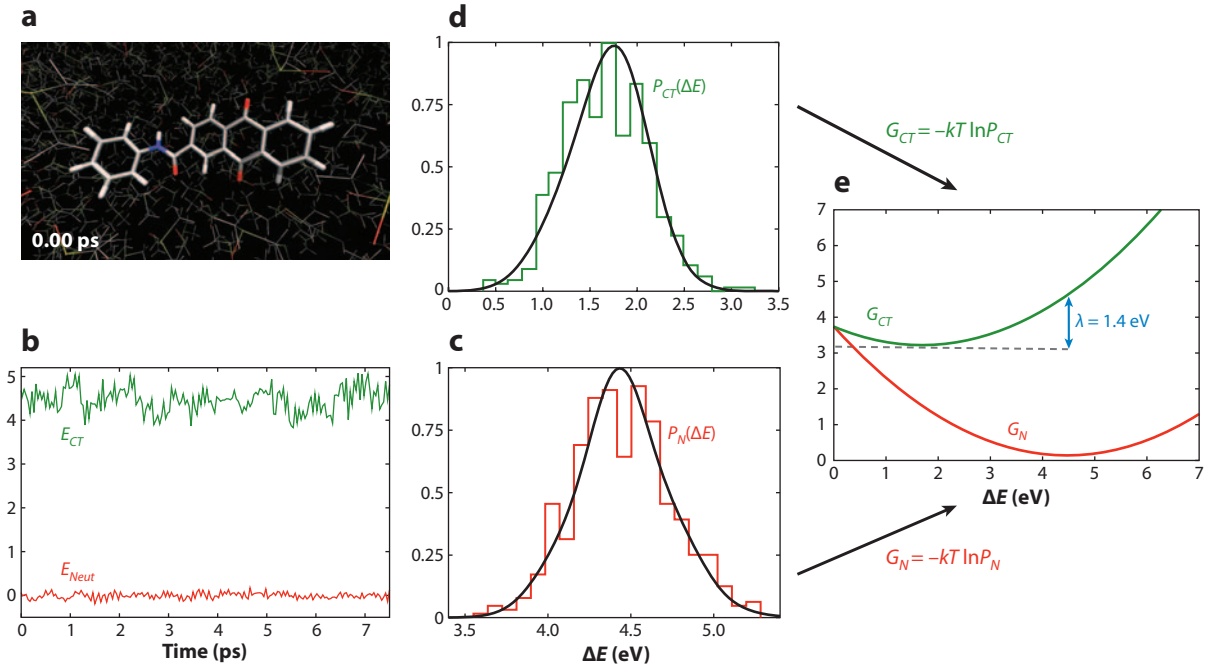

Figure 4

Sampling the electron transfer (ET) energy landscape with explicit solvent. (*a*) One first computes several long molecular dynamics trajectories, with the solute in either the neutral (pictured) or charge-transfer (CT) state. A movie of one such trajectory is available in the **Supplemental Material** (follow the **Supplemental Material link** from the Annual Reviews home page at **http://www.annualreviews.org**). (*b*) One monitors the energy of each diabat as a function of time and collects statistics on the energy gap ($\Delta E = E_{CT} - E_N$) from the (*c*) neutral and (*d*) CT trajectories. Here, the histograms show accumulated data, and the lines are a maximum likelihood fit. (*e*) Finally, the free energy, *G*, of each state is obtained from the log of the probability computed in panels *c* and *d*. All energies are in electron volts.

Finally, the free-energy surfaces can be obtained from

$$G_X(\Delta E) \equiv -kT \ln P_X(\Delta E) \quad X = CT \text{ or } N. \tag{17}$$

Figure 4*e* presents a simplified fit of this type wherein G_N and G_{CT} are assumed parabolic with the same curvature. Under these circumstances, G_N and G_{CT} are determined entirely by ΔG and λ, facilitating a direct comparison to the Marcus picture. We find that $\Delta G \approx 3.1$ eV for FAAQ, which is too high compared with experiment, primarily because a small basis (3-21G) has been used for the electronic structure. It is anticipated that similar simulations in a 6-31G* basis would be more in line with experiment. Meanwhile, we obtain $\lambda \approx 1.4$ eV—which is in excellent agreement with experiment ($\lambda \approx 1.41$ eV). A larger basis would likely have little effect on λ because it primarily reflects the geometry of the system, which should be less sensitive to the electronic basis. It thus appears that implicit models offer a fast and reasonably accurate means of predicting equilibrium properties of the diabats (such as ΔG), but that they should be supplemented by explicit solvent when out-of-equilibrium behavior (such as reorganization) is of interest.

5.2. Chemical Reactions

CDFT-CI: constrained density functional theory–configuration interaction

The diabatic picture employed for ET can also be applied to more general reactions. Instead of "donor" and "acceptor" electronic states, "product" and "reactant" diabats that exist at all points along the reaction coordinate are posited. This diabatic framework is the basis of empirical VB theory (16, 17) and has been used to analyze S_N1 (46) and S_N2 (112) reactions, as well as proton transfer (21). Once the diabatic states are defined, one is typically interested in computing the corresponding adiabatic energies by solving the generalized eigenvalue problem in Equation 10 at every nuclear configuration. Activation energies and transition pathways can then be predicted, and the transition-state electronic structure can be decomposed into reactant and product contributions. In this section, we briefly touch on some recent work in our group that attempts a systematic description of a wide range of reactions using the reactant/product division within CDFT (113).

The first step is to construct the reactant and product diabatic states. The task at hand is more challenging than it is for ET because in a typical chemical reaction, atoms are exchanged between the reactant and product molecules. Thus, whereas one can reasonably bin atoms as part of the donor or the acceptor fragment in an ET reaction, the same is not generally true in an S_N2 reaction, for example. This obstacle can be overcome if one assumes that the reactant state density resembles the superposition of the densities of the reactants (113, 114). To be concrete, suppose one is interested in a nucleophilic substitution reaction:

$$ClCH_3 + F^- \rightleftharpoons [Cl \cdots CH_3 \cdots F]^- \rightleftharpoons Cl^- + CH_3F.$$

Clearly, the reactant state should formally have zero charge ($q = 0$) and no net spin ($S = 0$) on the $ClCH_3$ group and [$q = -1$, $S = 1/2$] on F^-. Likewise, the product state should have Cl ($q = -1$, $S = 1/2$) and CH_3F ($q = 0$, $S = 0$). Now, we realize that the formal charges and spins will be precise when the fragments are well-separated, but these values are not expected to be accurate constraints at the transition state, where the fragments overlap significantly.

To obtain the correct constraint values for the reactant state (an equivalent procedure is followed for the product), one generates a promolecule density $\tilde{\rho}_R$ by superimposing the densities of $ClCH_3$ and F^-, calculated separately with their formal charges and spins and at the same level of theory as the final calculation; i.e.,

$$\tilde{\rho}_R^\sigma(\mathbf{r}) = \rho_{ClCH_3}^\sigma(\mathbf{r}) + \rho_{F^-}^\sigma(\mathbf{r}) \quad (\sigma = \alpha, \beta). \tag{18}$$

We note that the $ClCH_3$ fragment internal geometry is identical to the geometry of said fragment within the full calculation. The reactant charge and spin constraints of a given fragment ($X = ClCH_3$, F^-) are then obtained from $\tilde{\rho}_R$ using the weight function, w_X, associated with the same fragment. Thus

$$q_X = \int w_X(\mathbf{r})[\tilde{\rho}_R^\alpha(\mathbf{r}) + \tilde{\rho}_R^\beta(\mathbf{r})]d\mathbf{r}, \qquad S_X = \int w_X(\mathbf{r})[\tilde{\rho}_R^\alpha(\mathbf{r}) - \tilde{\rho}_R^\beta(\mathbf{r})]d\mathbf{r}. \tag{19}$$

q_X and S_X are then used in a CDFT calculation to build the desired reactant state, as illustrated in **Figure 5**.

This diabatic procedure generalizes to any AB + C → A + BC reaction. Furthermore, solving Equation 10 typically gives better adiabatic reaction barrier heights than those obtained from the unconstrained ground state, as illustrated in **Table 1**. Here, we consider the standard set of reaction barriers collected by Truhlar and coworkers (115) using both standard DFT and the CDFT-CI energy of Equation 10 using the diabatic prescription described above for reactant and product states. We see that the CDFT-CI results are typically significantly better than their

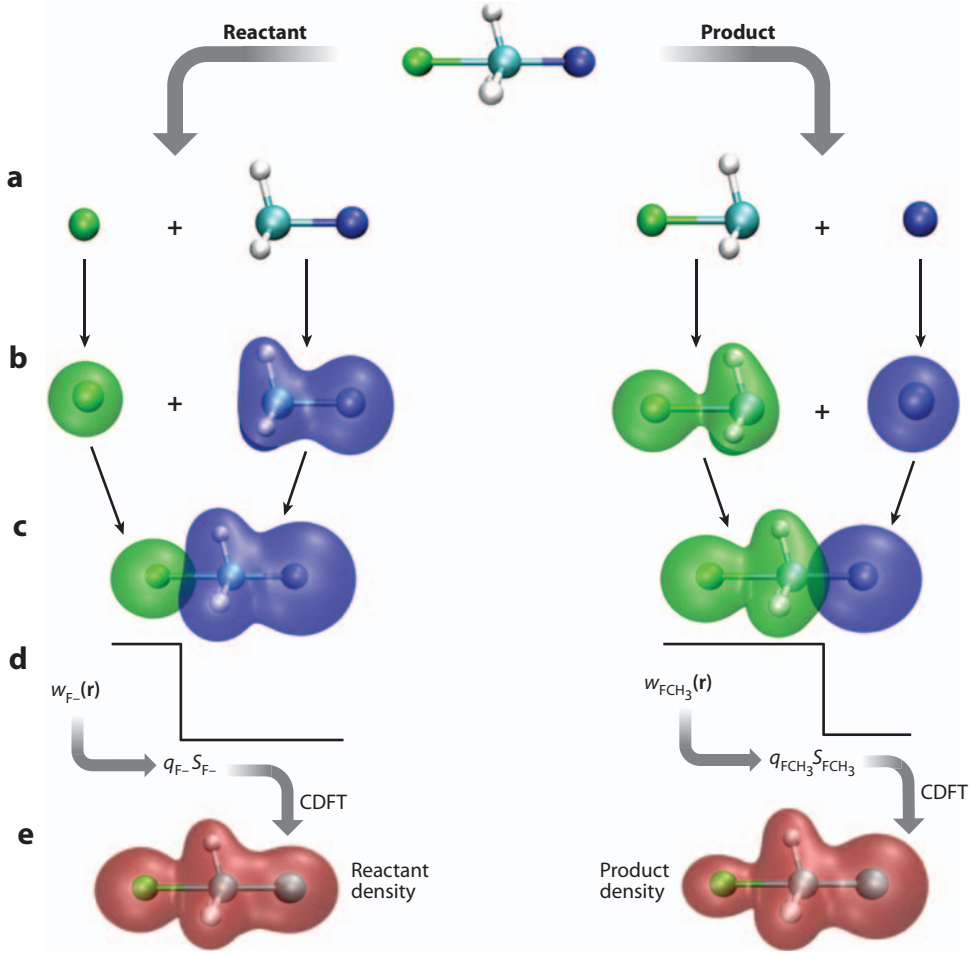

Figure 5

Constructing reactant and product diabatic states for $F^- + CH_3\,Cl \leftrightarrow FCH_3 + Cl^-$. (*a*) The atoms are divided according to the reactants and products. (*b*) DFT calculations are performed on the isolated fragments. (*c*) The fragment densities are added together. (*d*) The apparent charge (q) and spin (S) for each fragment are determined by integrating the population weight function $w_i(\mathbf{r})$ against the summed densities. (*e*) Constrained DFT calculations are performed with the computed q and S constraints to arrive at the reactant and product diabats.

unconstrained counterparts, particularly with less accurate functionals (113). Only for B97-2, which already gives fairly accurate barrier heights, do the limitations of our diabatic prescription become apparent. The clear improvement in the CDFT-CI barrier heights can be traced to two sources. First, a large fraction of the error in DFT barrier-height predictions is known to arise from electron self-interaction error (116, 117). Because the constraints force the electrons to localize in each of the underlying diabatic states, the effects of self-interaction error on the CDFT-CI results are mitigated (61, 63), improving the barrier heights. Second, by including a small CI within the calculation, CDFT-CI is able to include some of the static correlation that is missing in standard functionals (118), leading to a more stable description of bond breaking at the transition state.

Table 1 Summary of the mean absolute error (MAE) of barrier heights

	PBE		B3LYP		B97-2	
	Hydrogen transfer (36)					
MAE	9.7	**3.8**	4.6	**3.0**	3.6	**4.0**
	Heavy atom transfer (12)					
MAE	14.9	**7.6**	8.5	**2.3**	3.4	**4.7**
	Nucleophilic substitution (16)					
MAE	6.9	**2.3**	3.4	**1.3**	1.4	**2.9**
	All (63)					
MAE	10.0	**4.2**	5.1	**2.5**	3.0	**3.9**

The numbers in parenthesis represent the total number of barrier heights in each data set. Boldfaced numbers are CDFT-CI results. All energies are in kcal mol^{-1}.

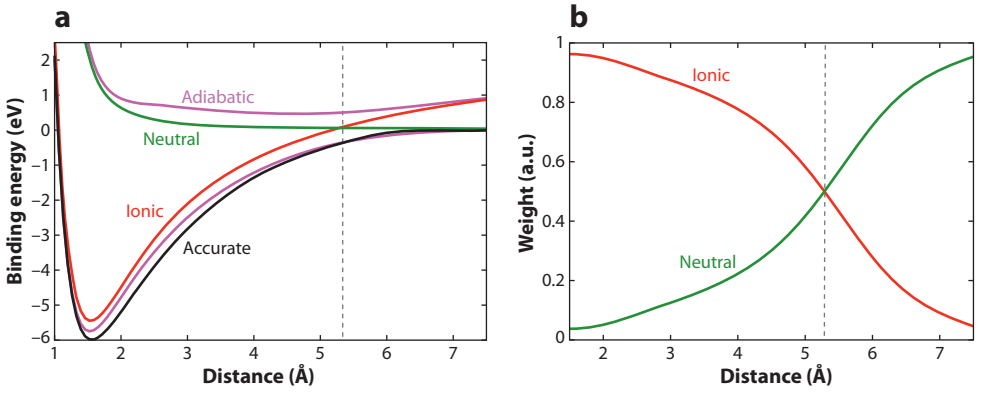

Figure 6

(*a*) Dissociation curves of LiF with various approximate methods. (*b*) Weights of configurations in the CDFT-CI (B3LYP) ground state. The ground state rapidly switches from neutral to ionic at the capture radius for Li^+F^- ($R = 5.4$ Å).

Importantly, this same diabatic prescription can be used not only to obtain accurate results, but to physically interpret the results as well. For example, we can use the same CDFT-CI approach to treat bonding in LiF if we consider four diabatic states: Li^+F^-, $Li^{\uparrow}F^{\downarrow}$, $Li^{\downarrow}F^{\uparrow}$, and Li^-F^+. This prescription gives an accurate description of the adiabatic dissociation curve (see **Figure 6**) when compared to a high-level OD(2) calculation (119, 120). However, the CDFT-CI calculation also allows us to break the adiabatic state down into contributions from the various ionic and covalent contributions. Thus we see that LiF is indeed primarily covalent beyond the capture radius of 5.4 Å, but that Li^+F^- becomes dominant as the bond becomes shorter.

6. CONCLUSIONS

In this review we briefly highlight the role diabatic states have in our qualitative understanding of chemistry, as well as the fundamental equations that allow diabats to be used for quantitative prediction. The nonexistence of strictly diabatic states leads to a variety of essentially diabatic states, each of which can be an appropriate description of chemistry under the right circumstances. For concreteness, we focus here on the use of density constraints for the definition of diabats and show

how the electronic energy, nuclear forces, and diabatic coupling can be obtained in this particular representation. We also illustrate how these diabatic states can be used for both the description of ET chemistry and the prediction of reaction barrier heights.

Moving forward, we see an expanding role for diabatic states in the area of reaction dynamics—in particular, excited-state dynamics. Constructive strategies such as VB or CDFT techniques offer direct access to diabatic potential energy surfaces without recourse to the corresponding adiabats. Thus, energies, forces, and molecular properties can easily be computed on the fly, facilitating molecular dynamics simulation of large systems. Thus, in the case of ET, one is already able to propagate trajectories on individual diabatic surfaces to sample the free-energy landscape (see **Figure 4**) even when one of those states is not the ground state.

Even without any further theoretical advances (see Future Issues) in our understanding of diabatic states, the existing technology is well-positioned to answer important chemical questions. The applications presented here are necessarily by way of illustration and validation of the concepts involved. However, the same steps outlined above could be used in the description of ultrafast photoinduced ET in solution (121) or at interfaces (122), as well as in the description of reaction barriers in electrochemical (123), photovoltaic (124), and photosynthetic (125) architectures. Thus, we see that although diabatic states have their historical origins in the qualitative description of chemistry, these same states promise to play an active role in the future of computational and theoretical chemistry.

SUMMARY POINTS

1. Diabatic states provide an intuitive means of describing bonding by, for example, decomposing the wave function into ionic and covalent contributions.
2. Diabats provide smooth potential energy surfaces that correspond to well-defined product and reactant channels.
3. Mathematically, one cannot construct a set of strictly diabatic states out of a set of adiabats. As a result, there are many approximate prescriptions for diabats available to chemists.
4. Constructive approaches facilitate the application of diabatic states in on-the-fly dynamics.
5. CDFT provides a practical constructive route for obtaining approximate diabats in large molecular systems.
6. Diabatic states provide a framework for obtaining quantitative predictions about ET dynamics and chemical reaction rates.

FUTURE ISSUES

1. It would be ideal to develop a less arbitrary construction of diabatic states that is still computationally inexpensive. At present, CDFT requires the identification of fragments and the (nonunique) choice of atomic populations. A prescription that automatically optimizes the fragment choice and the atomic populations based on energy minimization would clearly be preferable. In this area, the ideas of partition theory (126, 127) might provide a way forward.

2. The results obtained so far indicate CDFT-CI gives accurate adiabatic ground-state potential energy surfaces. The CI eigenequation (Equation 10) also provides excited states. Under what circumstances are the excitation energies accurate?
3. It would be beneficial to generate trajectories that allow quantum transitions between the diabatic electronic states. These simulations could employ, for example, surface hopping (128), multiple spawning (129), or generalized Langevin (130) techniques to describe the quantum transitions. Simulations of this type would be instrumental in directly predicting ET kinetics from the dynamics.

DISCLOSURE STATEMENT

The authors are not aware of any affiliations, memberships, funding, or financial holdings that might be perceived as affecting the objectivity of this review.

ACKNOWLEDGMENTS

This work was sponsored by an NSF-CAREER Award (CHE-0547877). T.V. gratefully acknowledges a Packard Fellowship and a Sloan Fellowship.

LITERATURE CITED

1. **Köppel H, Domcke W, Cederbaum LS. 1984. Multimode molecular dynamics beyond the Born-Oppenheimer approximation. *Adv. Chem. Phys.* 57:59–246**
2. Manthe U, Köppel H. 1990. Dynamics on potential energy surfaces with a conical intersection: adiabatic, intermediate, and diabatic behavior. *J. Chem. Phys.* 93:1658–69
3. Kim Y, Corchado JC, Villà J, Xing J, Truhlar DG. 2000. Multiconfiguration molecular mechanics algorithm for potential energy surfaces of chemical reactions. *J. Chem. Phys.* 112:2718–35
4. Liyanage R, Gordon R, Field R. 1998. Diabatic analysis of the electronic states of hydrogen chloride. *J. Chem. Phys.* 109:8374–87
5. Mueller J, Morton M, Curry S, Abbatt J, Butler L. 2000. Intersystem crossing and nonadiabatic product channels in the photodissociation of N_2O_4 at 193 nm. *J. Phys. Chem. A* 104:4825–32
6. Ichino T, Gianola AJ, Lineberger WC, Stanton JF. 2006. Nonadiabatic effects in the photoelectron spectrum of the pyrazolide-d_3 anion: three-state interactions in the pyrazolyl-d_3 radical. *J. Chem. Phys.* 125:084312
7. Gadéa FX, Pélissier M. 1990. Approximately diabatic states: a relation between effective Hamiltonian techniques and explicit cancellation of the derivative coupling. *J. Chem. Phys.* 93:545–51
8. Nakamura H. 1991. What are the basic mechanisms of eletronic transitions in molecular dynamic processes? *Int. Rev. Phys. Chem.* 10:123–88
9. Woywod C, Stengle M, Domcke W, Flöthmann H, Schinke R. 1997. Photodissociation of ozone in the Chappuis band. I. Electronic structure calculations. *J. Chem. Phys.* 107:7282–95
10. Müller U, Stock G. 1997. Surface-hopping modeling of photoinduced relaxation dynamics on coupled potential-energy surfaces. *J. Chem. Phys.* 107:6230–45
11. Butler LJ. 1998. Chemical reaction dynamics beyond the Born-Oppenheimer approximation. *Annu. Rev. Phys. Chem.* 49:125–71
12. Cohen JM, Micha DA. 1992. Electronically diabatic atom-atom collisions: a self-consistent eikonal approximation. *J. Chem. Phys.* 97:1038–52
13. Tully JC. 2000. Chemical dynamics at metal surfaces. *Annu. Rev. Phys. Chem.* 51:153–78
14. Mahapatra S, Koppel H, Cederbaum LS. 2001. Reactive scattering dynamics on conically intersecting potential energy surfaces: the $H + H_2$ exchange reaction. *J. Phys. Chem. A* 105:2321–29

1. Presents an extensive introduction to the use of diabatic states in modeling vibronic dynamics.

15. An enduring classic, highlights the important contributions of the VB picture of chemical binding.

16. Many years ahead of its time, introduces the empirical VB concept.

19. Presents a broad review of the relevance of ET in chemistry and biology.

15. Pauling L. 1960. *The Nature of the Chemical Bond*. Ithaca, NY: Cornell Univ. Press. 3rd ed.

16. Warshel A, Weiss RM. 1980. An empirical valence bond approach for comparing reactions in solutions and in enzymes. *J. Am. Chem. Soc.* 102:6218–26

17. Åqvist J, Warshel A. 1993. Simulation of enzyme reactions using valence-bond force fields and other hybrid quantum-classical approaches. *Chem. Rev.* 93:2523–44

18. Sidis V. 1992. Diabatic potential-energy surfaces for charge-transfer processes. *Adv. Chem. Phys.* 82:73–134

19. Marcus RA, Sutin N. 1985. Electron transfers in chemistry and biology. *Biochim. Biophys. Acta* 811:265–322

20. Timoneda JJI, Hynes JT. 1991. Nonequilibrium free energy surfaces for hydrogen-bonded proton-transfer complexes in solution. *J. Chem. Phys.* 95:10431–42

21. Hammes-Schiffer S, Tully JC. 1994. Proton transfer in solution: molecular dynamics with quantum transitions. *J. Chem. Phys.* 101:4657–67

22. Kuznetsov AM, Ulstrup J. 1999. Proton and hydrogen atom tunnelling in hydrolytic and redox enzyme catalysis. *Can. J. Chem.* 77:1085–96

23. Mead CA, Truhlar DG. 1982. Conditions for the definition of a strictly diabatic electronic basis for molecular systems. *J. Chem. Phys.* 77:6090–98

24. Baer M. 1975. Adiabatic and diabatic representations for atom-molecule collisions: treatment of the collinear arrangement. *Chem. Phys. Lett.* 35:112–18

25. Baer M. 1980. Electronic non-adiabatic transitions: derivation of the general adiabatic-diabatic transformation matrix. *Mol. Phys.* 40:1011–13

26. Baer M, Englman R. 1992. A study of the diabatic electronic representation within the Born-Oppenheimer approximation. *Mol. Phys.* 75:293–303

27. Pacher T, Cederbaum LS, Köppel H. 1993. Adiabatic and quasidiabatic states in a gauge theoretical framework. *Adv. Chem. Phys.* 84:293–391

28. Pacher T, Cederbaum LS, Köppel H. 1988. Approximately diabatic states from block diagonalization of the electronic Hamiltonian. *J. Chem. Phys.* 89:7367–81

29. Pacher T, Köppel H, Cederbaum LS. 1991. Quasidiabatic states from ab initio calculations by block diagonalization of the electronic Hamiltonian: use of frozen orbitals. *J. Chem. Phys.* 95:6668–80

30. Pacher T, Mead CA, Cederbaum LS, Köppel H. 1989. Gauge theory and quasidiabatic states in molecular physics. *J. Chem. Phys.* 91:7057–62

31. Ruedenberg K, Atchity GJ. 1993. A quantum-chemical determination of diabatic states. *J. Chem. Phys.* 99:3799–803

32. Atchity GJ, Ruedenberg K. 1997. Determination of diabatic states through enforcement of configurational uniformity. *Theor. Chem. Acc.* 97:47–58

33. Thiel A, Köppel H. 1999. Proposal and numerical test of a simple diabatization scheme. *J. Chem. Phys.* 110:9371–83

34. Köppel H, Gronki J, Mahapatra S. 2001. Construction scheme for regularized diabatic states. *J. Chem. Phys.* 115:2377–88

35. Nakamura H, Truhlar DG. 2001. The direct calculation of diabatic states based on configurational uniformity. *J. Chem. Phys.* 115:10353–72

36. Nakamura H, Truhlar DG. 2002. Direct diabatization of electronic states by the fourfold way. II. Dynamical correlation and rearrangment processes. *J. Chem. Phys.* 117:5576–93

37. Mulliken R. 1952. Molecular compounds and their spectra. II. *J. Am. Chem. Soc.* 74:811–24

38. Hush N. 1967. Intervalence-transfer absorption. Part 2. Theoretical considerations and spectroscopic data. *Prog. Inorg. Chem.* 8:391–444

39. Cave RJ, Newton MD. 1996. Generalization of the Mulliken-Hush treatment for the calculation of electron transfer matrix elements. *Chem. Phys. Lett.* 249:15–19

40. Cave RJ, Newton MD. 1997. Calculation of electronic coupling matrix elements for ground and excited state electron transfer reactions: comparison of the generalized Mulliken-Hush and block diagonalization methods. *J. Chem. Phys.* 106:9213–26

41. Werner HJ, Meyer W. 1981. MCSCF study of the avoided curve crossing of the two lowest $^1\sigma_+$ states of LiF. *J. Chem. Phys.* 74:5802–7

42. Boys SF. 1960. Construction of some molecular orbitals to be approximately invariant for changes from one molecule to another. *Rev. Mod. Phys* 32:296–99
43. Subotnik JE, Yeganeh S, Cave RJ, Ratner MA. 2008. Constructing diabatic states from adiabatic states: extending generalized Mulliken Hush to multiple charge centers with Boys localization. *J. Chem. Phys.* 129:244101
44. Truhlar DG. 2007. Valence bond theory for chemical dynamics. *J. Comp. Chem.* 28:73–86
45. Song LC, Gao JL. 2008. On the construction of diabatic and adiabatic potential energy surfaces based on ab initio valence bond theory. *J. Phys. Chem. A* 112:12925–35
46. Kim HJ, Hynes JT. 1992. A theoretical model for S_N1 ionic dissociation in solution. 1. Activation free energetics and transition state structure. *J. Am. Chem. Soc.* 114:10508–28
47. Soudackov A, Hammes-Schiffer S. 2000. Derivation of rate expressions for nonadiabatic proton-coupled electron transfer reactions in solution. *J. Chem. Phys.* 113:2385–96
48. Mo YR, Gao JL. 2000. An ab initio molecular orbital-valence bond (MOVB) method for simulating chemical reactions in solution. *J. Phys. Chem. A* 104:3012–20
49. Gerratt J, Cooper DL, Karadakov PB, Raimondi M. 1997. Modern valence bond theory. *Chem. Soc. Rev.* 26:87–100
50. Wesolowski TA, Warshel A. 1993. Frozen density-functional approach for ab initio calculations of solvated molecules. *J. Phys. Chem.* 97:8050–53
51. Olsson MHM, Hong GY, Warshel A. 2003. Frozen density functional free energy simulations of redox proteins: computational studies of the reduction potential of plastocyanin. *J. Am. Chem. Soc.* 2003:5025–39
52. Dederichs PH, Blügel S, Zeller R, Akai H. 1984. Ground states of constrained systems: application to cerium impurities. *Phys. Rev. Lett.* 53:2512–15
53. Okamoto K, Hasobe T, Tkachenko NV, Lemmetyinen H, Kamat PV, Fukuzimi S. 2005. Drastic difference in lifetimes of the charge-separated state of the formanilide-anthraquinone dyad versus the ferrocene-formanilide-anthraquinone triad and their photoelectrochemical properties of the composite films with fullerene clusters. *J. Phys. Chem. A* 109:4662–70
54. Wu Q, Van Voorhis T. 2006. Direct calculation of electron transfer parameters through constrained density functional theory. *J. Phys. Chem. A* 110:9212–18
55. Mulliken RS. 1955. Electronic populations analysis on LCAO-MO molecular wave functions. *J. Chem. Phys.* 23:1833–40
56. Löwdin PO. 1950. On the non-orthogonality problem connected with the use of atomic wave functions in the theory of molecules and crystals. *J. Chem. Phys.* 18:365–75
57. Bader RFW. 1985. Atoms in molecules. *Acc. Chem. Res.* 18:9–15
58. Becke AD. 1988. A multicenter numerical integration scheme for polyatomic molecules. *J. Chem. Phys.* 88:2547–53
59. Hirshfeld FL. 1977. Bonded-atom fragments for describing molecular charge densities. *Theor. Chem. Acc.* 44:129–38
60. Wu Q, Van Voorhis T. 2005. A direct optimization method to study constrained systems within density functional theory. *Phys. Rev. A* 72:024502
61. Wu Q, Van Voorhis T. 2006. Constrained density functional theory and its application in long range electron transfer. *J. Chem. Theor. Comp.* 2:765–74
62. Behler J, Delley B, Lorenz S, Reuter K, Scheffler M. 2005. Dissociation of O_2 at Al(111): the role of spin selection rules. *Phys. Rev. Lett.* 94:036104
63. Rudra I, Wu Q, Van Voorhis T. 2006. Accurate magnetic exchange couplings in transition metal complexes from constrained density functional theory. *J. Chem. Phys.* 24:024103
64. Rudra I, Wu Q, Van Voorhis T. 2007. Predicting exchange coupling constants in frustrated molecular magnets using density functional theory. *Inorg. Chem.* 46:10539–48
65. Behler J, Delley B, Reuter K, Scheffler M. 2007. Nonadiabatic potential-energy surfaces by constrained density-functional theory. *Phys. Rev. B* 75:115409
66. High Performance Computational Chemistry Group. 2004. *NWChem, A Computational Chemistry Package for Parallel Computers, Version 5.0*. Richland, WA: Pacific Northwest Natl. Lab.

44. Gives a unique perspective on the role of VB in chemistry.

54. Presents the connection between CDFT and ET.

67. Shao Y, Molanr LF, Jung Y, Kussmann J, Ochsenfeld C, et al. 2006. Advances in methods and algorithms in a modern quantum chemistry program package. *Phys. Chem. Chem. Phys.* 8:3172–91
68. Becke AD. 1993. Density-functional thermochemistry 0.3. The role of exact exchange. *J. Chem. Phys.* 98:5648–52
69. Klamt A, Schuurmann G. 1993. COSMO—a new approach to dielectric screening in solvents with explicit expressions for the screening energy and its gradient. *J. Chem. Soc. Perkins Trans. 2* 5:799–805
70. Rehm D, Weller A. 1970. Kinetics of fluorescence quenching by electron transfer and H-atom transfer. *Israel J. Chem.* 8:259–71
71. Siders P, Cave RJ, Marcus RA. 1984. Model for orientation effects in electron transfer reactions. *J. Chem. Phys.* 81:5613–24
72. Daizadeh I, Medvedev ES, Stuchebrukhov AA. 1997. Effect of protein dynamics on biological electron transfer. *Proc. Natl. Acad. Sci. USA* 94:3703–8

73. Introduces the definition of the diabatic coupling in CDFT.

73. Wu Q, Van Voorhis T. 2006. Extracting electron transfer coupling elements from constrained density functional theory. *J. Chem. Phys.* 125:164105
74. Watchers AJH. 1970. Gaussian basis set for molecular wavefunctions containing third-row atoms. *J. Chem. Phys.* 52:1033–36

75. Gives an approachable introduction to ET in chemical physics.

75. Barbara PF, Meyer TJ, Ratner MA. 1996. Contemporary issues in electron transfer research. *J. Phys. Chem.* 100:13148–68
76. Barbara PF, Jarzeba W. 1990. Ultrafast photochemical intramolecular charge transfer and excited state solvation. *Adv. Photochem.* 15:1–68
77. Marcus RA. 1964. Chemical and electrochemical electron-transfer theory. *Annu. Rev. Phys. Chem.* 15:155–96
78. Kestner NR, Logan J, Jortner J. 1974. Thermal electron transfer reactions in polar solvents. *J. Phys. Chem.* 78:2148–66
79. Small DW, Matyushov DV, Voth GA. 2003. The theory of electron transfer reactions: What may be missing? *J. Am. Chem. Soc.* 125:7470–78
80. Hush NS. 1961. Adiabatic theory of outer sphere electron-transfer reactions in solution. *Trans. Faraday Soc.* 57:557–80
81. Jortner J. 1976. Temperature dependent activation energy for electron transfer between biological molecules. *J. Chem. Phys.* 64:4860–67
82. Sit PHL, Cococcioni M, Marzari N. 2006. Realistic quantitative descriptions of electron transfer reactions: diabatic free-energy surfaces from first-principles molecular dynamics. *Phys. Rev. Lett.* 97:028303
83. Oberhofer H, Blumberger J. 2009. Charge constrained density functional molecular dynamics for simulation of condensed phase electron transfer reactions. *J. Chem. Phys.* 131:064101
84. Marcus RA. 1956. On the theory of oxidation-reduction reactions involving electron transfer. I. *J. Chem. Phys.* 24:966–78
85. Carter EA, Hynes JT. 1991. Solvation dynamics for an ion pair in a polar solvent: time-dependent fluorescence and photochemical charge transfer. *J. Chem. Phys.* 94:5961–79
86. Hwang JK, Warshel A. 1987. Microscopic examination of free-energy relationships for electron-transfer in polar solvents. *J. Am. Chem. Soc.* 109:715–20
87. Tachiya M. 1989. Relation between the electron-transfer rate and the free energy change of reaction. *J. Phys. Chem.* 93:7050–52
88. Subotnik JE, Cave RJ, Steele RP, Shenvi N. 2009. The initial and final states of electron and energy transfer processes: diabatization as motivated by system-solvent interactions. *J. Chem. Phys.* 130:234102
89. Onsager L. 1936. Electric moments of molecules in liquids. *J. Am. Chem. Soc.* 58:1486–93
90. Rinaldi D, Ruiz-Lopez MF, Rivail JL. 1983. Ab initio SCF calculations on electrostatically solvated molecules using a deformable three axes ellipsoidal cavity. *J. Chem. Phys.* 78:834–38
91. Barone V, Cossi M. 1998. Quantum calculation of molecular energies and energy gradients in solution by a conductor solvent model. *J. Phys. Chem. A* 102:1995–2001
92. Cramer CJ, Truhlar DG. 1999. Implicit solvation models: equilibria, structure, spectra, and dynamics. *Chem. Rev.* 99:2161–200
93. Hsu CP, Song X, Marcus RA. 1997. Time-dependent Stokes shift and its calculation from solvent dielectric dispersion data. *J. Phys. Chem. B* 101:2546–51

94. Cramer CJ, Truhlar DG. 1992. An SCF solvation model for the hydrophobic effect and absolute free energies of aqueous solvation. *Science* 256:213–17
95. Aguilar MA. 2001. Separation of the electric polarization into fast and slow components: comparison of two partition schemes. *J. Phys. Chem. A* 105:10393–96
96. Mennucci B, Tomasi J. 1997. Continuum solvation models: a new approach to the problem of solute's charge distribution and cavity boundaries. *J. Chem. Phys.* 106:5151–58
97. Cossi M, Barone V. 2000. Solvent effect on vertical electronic transitions by the polarizable continuum model. *J. Chem. Phys.* 112:2427–35
98. Warshel A. 1982. Dynamics of reactions in polar solvents: semi-classical trajectory studies of electron-transfer and proton-transfer reactions. *J. Phys. Chem.* 86:2218–24
99. Warshel A, Hwang JK. 1986. Simulation of the dynamics of electron-transfer reactions in polar solvents: semiclassical trajectories and dispersed polaron approaches. *J. Chem. Phys.* 84:4938–57
100. Zichi DA, Ciccotti G, Hynes JT, Ferrario M. 1989. Molecular dynamics simulation of electron-transfer reactions in solution. *J. Phys. Chem.* 93:6261–65
101. King G, Warshel A. 1990. Investigation of the free-energy functions for electron transfer reactions. *J. Chem. Phys.* 93:8682–92
102. Kuharski RA, Bader JS, Chandler D, Sprik M, Klein ML, Impey RW. 1988. Molecular model for aqueous ferrous-ferric electron transfer. *J. Chem. Phys.* 89:3248–57
103. Bader RS, Kuharski RA, Chandler D. 1990. Role of nuclear tunneling in aqueous ferrous-ferric electron transfer. *J. Chem. Phys.* 93:230–36
104. Bader RS, Chandler D. 1989. Computer simulation of photochemically induced electron transfer. *Chem. Phys. Lett.* 157:501–4
105. Blumberger J, Sprik M. 2005. Ab initio molecular dynamics simulation of the aqueous Ru^{2+}/Ru^{3+} redox reaction: the Marcus perspective. *J. Phys. Chem. B* 109:6793–804
106. Tateyama Y, Blumberger J, Sprik M, Tavernelli I. 2005. Density-functional molecular dynamics study of the redox reactions of two anionic, aqueous transition-metal complexes. *J. Chem. Phys.* 122:234505
107. Blumberger J, Sprik M. 2006. Quantum versus classical electron transfer energy as reaction coordinate for the aqueous Ru^{2+}/Ru^{3+} redox reaction. *Theor. Chem. Acc.* 115:113–26
108. VandeVondele J, Lynden-Bell R, Meijer EJ, Sprik M. 2006. Density functional theory study of tetrathiafulvalene and thianthrene in acetonitrile: structure, dynamics, and redox properties. *J. Phys. Chem. B* 110:3614–23
109. VandeVondele J, Ayala R, Sulpizi M, Sprik M. 2007. Redox free energies and one-electron energy levels in density functional theory based ab initio molecular dynamics. *J. Electroanal. Chem.* 607:113–20
110. Kowalczyk T, Wang LP, Van Voorhis T. 2009. In preparation.
111. Sulpizi M, Raugei S, VandeVondele J, Carloni P, Sprik M. 2007. Calculation of redox properties: understanding short- and long-range effects in rubredoxin. *J. Phys. Chem. B* 111:3969–76
112. Mo YR, Gao JL. 2000. Ab initio QM/MM simulations with a molecular orbital-valence bond (MOVB) method: application to an S_N2 reaction in water. *J. Comp. Chem.* 21:1458–69
113. Wu Q, Kaduk B, Van Voorhis T. 2009. Constrained density functional theory based configuration interaction improves the prediction of barrier heights. *J. Chem. Phys.* 130:034109
114. Wu Q, Cheng CL, Van Voorhis T. 2007. Configuration interaction based on constrained density functional theory. *J. Chem. Phys.* 127:164119
115. Zhao Y, Gonzalez-Garcia N, Truhlar DG. 2005. Benchmark database of barrier heights for heavy atom transfer, nucleophilic substitution, association, and unimolecular reactions and its use to test theoretical methods. *J. Phys. Chem. A* 109:2012–18
116. Vydrov OA, Scuseria GE. 2006. Assessment of a long-range corrected hybrid functional. *J. Chem. Phys.* 125:234109
117. Janesko BG, Scuseria GE. 2008. Hartree-Fock orbitals significantly improve the reaction barrier heights predicted by semilocal density functionals. *J. Chem. Phys.* 128:244112
118. Cremer D. 2001. Density functional theory: coverage of dynamic and non-dynamic electron correlation effects. *Mol. Phys.* 99:1899–940

119. Sherrill CD, Krylov AI, Byrd EFC, Head-Gordon M. 1998. Energies and analytic gradients for a coupled-cluster doubles model using variational Brueckner orbitals: application to symmetry breaking in O_4^+. *J. Chem. Phys.* 109:4171–81
120. Gwaltney SR, Head-Gordon M. 2000. A second-order correction to singles and doubles coupled-cluster methods based on a perturbative expansion of a similarity transformed Hamiltonian. *Chem. Phys. Lett.* 323:21–28
121. Maroncelli M, MacInnis J, Fleming GR. 1989. Polar-solvent dynamis and electron transfer reactions. *Science* 243:1674–81
122. Asbury JB, Hao E, Wang Y, Ghosh HN, Lian T. 2001. Ultrafast electron transfer dynamics from molecular adsorbates to semiconductor nanocrystalline thin films. *J. Phys. Chem. B* 105:4545–57
123. Grätzel M. 2001. Photoelectrochemical cells. *Nature* 414:338–44
124. Peumans P, Yakimov A, Forrest SR. 2003. Small molecular weight organic thin-film photodetectors and solar cells. *J. Appl. Phys.* 93:3693–723
125. Ferreira KN, Iverson TM, Maghlaoui K, Barber J, Iwata S. 2004. Architecture of the photosynthetic oxygen-evolving center. *Science* 303:1831–38
126. Cohen MH, Wasserman A. 2007. On the foundations of chemical reactivity theory. *J. Phys. Chem. A* 111:2229–42
127. Elliott P, Cohen MH, Wasserman A, Burke K. 2009. Density functional partition theory with fractional occupations. *J. Chem. Theor. Comp.* 5:827–33
128. Tully JC. 1990. Molecular dynamics with electronic transitions. *J. Chem. Phys.* 93:1061–71
129. Ben-Nun M, Quenneville J, Martinez TJ. 2000. Ab initio multiple spawning: photochemistry from first principles quantum molecular dynamics. *J. Phys. Chem. A* 104:5161–75
130. Song X, Wang HB, Van Voorhis T. 2008. A Langevin equation approach to electron transfer reactions in the diabatic basis. *J. Chem. Phys.* 129:144502

Annual Review of
Physical Chemistry
Volume 61, 2010

Contents

Indexes

Errata

An online log of corrections to *Annual Review of Physical Chemistry* articles may be found at http://physchem.annualreviews.org/errata.shtml